MESOMETEOROLOGY PROJECT

Department of the Geophysical Sciences
The University of Chicago

45p.

UNPUBLISHED PRELIMINARY DATA

SYNOPTIC INTERPRETATION OF TIROS III MEASUREMENTS OF INFRARED RADIATION

by

Finn Pedersen and Tetsuya Fujita

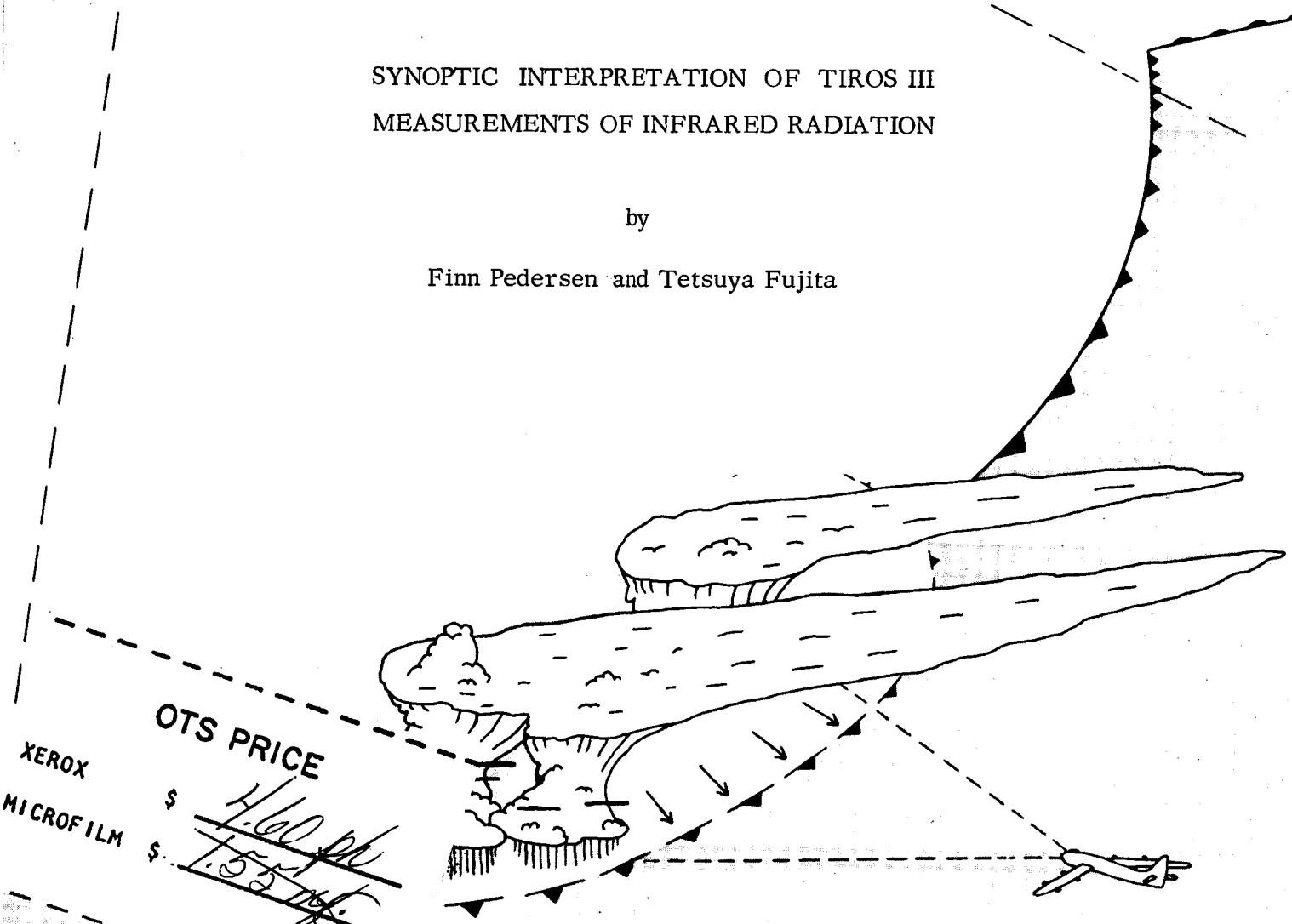

Research Paper #19
October 1963

MESOMETEOROLOGY PROJECT --------RESEARCH PAPERS

1. Report on the Chicago Tornado of March 4, 1961 - Rodger A. Brown and Tetsuya Fujita *

2. Index to the NSSP Surface Network - Tetsuya Fujita *

3. Outline of a Technique for Precise Rectification of Satellite Cloud Photographs - Tetsuya Fujita *

4. Horizontal Structure of Mountain Winds - Henry A. Brown *

5. An Investigation of Developmental Processes of the Wake Depression Through Excess Pressure Analysis of Nocturnal Showers - Joseph L. Goldman *

6. Precipitation in the 1960 Flagstaff Mesometeorological Network - Kenneth A. Styber *

7. On a Method of Single- and Dual-Image Photogrammetry of Panoramic Aerial Photographs - Tetsuya Fujita (To be published)

8. A Review of Researches on Analytical Mesometeorology - Tetsuya Fujita

9. Meteorological Interpretations of Convective Nephsystems Appearing in TIROS Cloud Photographs - Tetsuya Fujita, Toshimitsu Ushijima, William A. Hass, and George T. Dellert, Jr.

10. Study of the Development of Prefrontal Squall-Systems Using NSSP Network Data - Joseph L. Goldman

11. Analysis of Selected Aircraft Data from NSSP Operation, 1962 - Tetsuya Fujita

12. Study of a Long Condensation Trail Photographed by TIROS I - Toshimitsu Ushijima

13. A Technique for Precise Analysis of Satellite Data; Volume 1 - Photogrammetry - (Published as MSL Report No. 14) - Tetsuya Fujita

14. Investigation of a Summer Jet Stream Using TIROS and Aerological Data - Kozo Ninomiya

15. Outline of a Theory and Examples for Precise Analysis of Satellite Radiation Data - Tetsuya Fujita

* Out of Print

(Continued on back cover)

MESOMETEOROLOGY PROJECT

Department of the Geophysical Sciences

The University of Chicago U., Ill.
0624692

SYNOPTIC INTERPRETATION OF TIROS III MEASUREMENTS OF INFRARED RADIATION

by

Finn Pedersen* and Tetsuya Fujita Oct. 1963 45p refs

(NASA Grant NsG-333; ~~Weather Bur.~~ Grant Cwb WBG-6) Index

cite only
(NASA CR-53851; Res. Paper 19) OTS: See Cover

RESEARCH PAPER #19

This research was supported by the Meteorological Satellite Laboratory, United States Weather Bureau, under grant Cwb WBG-6, and partially by the National Aeronautic and Space Administration under grant NASA Nsg 333.

* On leave from the Norwegian Weather Service at Bergen.

TABLE OF CONTENTS

ABSTRACT

19604

Infrared radiation measurements in Channels 2 and 4 for R/O 142 and 143 are used for this study. The effects of large zenith angles of the radiometer axis on the recorded radiation patterns are discussed and illustrated by means of examples. The method of Wark, Yamamoto, and Lienesch for computing outgoing total infrared flux by means of Channel 4 measurements is further developed and given a form more suitable for work on maps. This method is tested by applying it to the initial and complemental scans of one and the same general area where the measurements are separated by a time interval of only a few minutes. The method is found to give reasonable and consistent mean values for areas, each of which covers about 0.2 percent of the area of the total surface of the earth.

Author

I. INTRODUCTION

The case study we present here is a night case; consequently, only those measurements in the infrared Channels 1, 2, and 4 were available. The material at our disposal was, on the one hand, The Attitude World Map of TIROS III, published by NASA, and, on the other hand the Brush Record Tape of the radiation. From the latter it was evident that the Channel 1 measurements were of questionable value for the two orbits which were used by us. Our study therefore includes only Channel 2 and Channel 4 measurements. Orbits 142 and 143 were flown on 22 July 1961: for Orbit 142 the radiation measurements we have used were performed during the time interval 0752-0801 GCT; for Orbit 143 the time was 0936-0947 GCT.

By comparing the nadir angles obtained from The Attitude World Map of TIROS III through the analysis technique developed by Fujita (1963a and 1963b) with nadir angles obtained from the open mode of the radiation records, we were able to get a very satisfactory determination of time and location for successive scans.

When, however, the signals from the satellite were translated into terms of effective black-body temperatures (Data User's Manual) and infrared fluxes, it soon became evident that these quantities were considerably smaller than would be expected. This turned out, according to information received from members of the NASA staff, to be due to a progressive degradation of the instruments during flight, which made invalid the code for the translation of signals. In a personal communication, W. Bandeen of the Goddard Space Flight Center kindly put at our disposal the probable values of the corrections which should be applied to the data we were treating.

Since one of our main objects was to get absolute values for the total infrared flux escaping to outer space from the top of the atmosphere, all our maps had to be redrawn. As they are now presented, our values for temperatures and fluxes obviously inspire more confidence than the values we obtained before the corrections were made.

We have, however, been warned that the corrections are only estimates of the effects of a complicated degradation mechanism, which is not yet fully understood. Some uncer - tainty, therefore, still exists in the corrected values. Presumably, though, they are the best that can be obtained at the present time.

II. THE SYNOPTIC SITUATION

The weather situation at the regular synoptic hour closest to the time of flight is shown in Fig. 1, which is a simplified copy of the U.S. Weather Bureau Surface Map for 22 July 1961, 0900 GCT. Only a few observations have been entered. Also shown on the map are the subpoint tracks for parts of Orbits 142 and 143, with times for the successive locations of the subpoints inserted. The approximate time interval between the two tracks is 100 minutes.

The shaded areas indicate the main regions with a complete overcast, as far as this could be ascertained from the regular network of synoptic stations. Fronts are indicated by the usual symbols. The main features of the weather situation are as follows: 1) a frontal zone stretching from the Great Lakes region southwestwards which separates a southeastern area of moist warm air (flowing northeastwards from the Gulf of Mexico) from cooler and drier air in the northwestern part of the continent; and 2) in connection with the fronts, two areas of low pressure, one located west of Lake Michigan and another in the Oklahoma-Kansas area. Later observations showed that the southwestern low was in a state of development, while the northeastern low gradually weakened in the course of the day. When we selected the case it was hoped that we would be able to cover the whole area of the northeastern low with radiation measurements taken at comparatively small zenith angles. Unfortunately, however, observations were discontinued for readout purposes; as a consequence, our radiation maps will cover only a part of the Great Lakes.

There are two main areas of complete overcast, each connected with one of the two lows mentioned above, as well as a narrow strip of overcast along the front between the lows. In both the main cloud areas scattered thunderstorms were reported. Another feature which stands out in the cloud distribution is the relatively cloud-free area situated north of the front joining the two lows.

All these features, it will be found, stand out clearly in the radiation maps as well. However, when comparing synoptic weather maps with radiation maps, there are some points which should be kept in mind. An exact correspondence between cold areas on the radiation maps and areas of overcast as observed from the ground is not to be expected. In overcast areas the satellite measurements in Channel 2, generally known as the "window region" of the water vapor spectrum, will register to a great extent the temperature of the upper boundary of the clouds; and this may vary considerably within the overcast areas. Adjacent areas with broken clouds will also appear in the radiation maps as comparatively cool areas, with effective black-body temperatures depending on the height and amount of clouds and also to some degree on the zenith angles through which the areas are viewed. Generally therefore, it will not be possible to trace the exact boundary of the overcast region from a map of infrared radiation alone. Further, more or less linear arrangement of clouds along a sloping frontal zone will appear on the radiation map as a cold tongue or as a linear arrangement of cold spots. The location of this arrangement on the radiation map will be determined mainly by the height of the upper surface of the clouds and cannot be expected to correspond exactly to the location of the surface front.

In the case of night observations there is the additional complication that it is often difficult for an observer on the ground to decide whether he is confronted with a clear sky, a thin haze, or a light cirrostratus. These various possibilities will manifest themselves in a rather different way depending upon the zenith angle of the radiometer beam.

On Fig. 2, also a U.S. Weather Bureau Map, is shown in more detail the distribution of cloud cover. Over the western mountain region a large, clear area is evident; since ours is a night case one should expect that the elevation of the mountain ranges will show up to some extent in the radiation patterns. The warm air coming up from the Gulf has, likewise, a large area comparatively free from clouds. On the coast of Louisiana there is an overcast area, probably due to storms drifting in with the onshore winds from the Gulf. Finally, in Mexico there is also a fairly large area with overcast conditions.

Fig. 3 is a slightly simplified reproduction of the U.S. Weather Bureau Map for the 300-mb surface, 22 July 1961, 1200 GCT. Only a few observations have been plotted. For our purpose the main feature to be noticed is the strong upper winds southeast of the upper low and roughly parallel to the front. The existence of these upper winds explains the extension towards the northeast of the large overcast area connected with the Oklahoma-Kansas low. The clear or relatively cloud-free strip parallel to the front is obviously due to subsiding motions in the region between the two surface lows.

III. THE ANGULAR RESOLUTION OF THE RADIOMETER

One of the first questions that has to be taken into consideration, when one intends to use the radiation measurements for the mapping of synoptic systems, is that concerning the resolution of the radiometers. Some information on this subject has been given by Fujita (1963a) and is the basis for the following considerations.

With a vertical radiometer axis the scan spot has a circular contour. For increasing zenith angles of the radiometer axis the scan spots become increasingly elongated but can still be considered as elipses up to zenith angles of about 70 deg. For still larger zenith angles contamination from outer space sets in and makes the immediate application of the data more or less illusory for many purposes.

In the sections of the two orbits that are treated here the height of the satellite was very close to 750 km. If we define as a scan spot the area from which the radiometer will receive 80 percent of the recorded energy from a uniformly illuminated surface, we get for a satellite height of 750 km the values cited in the table below. Figs. 4, 5, 6, and 7, in which actual scan spots for our case are indicated in their proper location, should also be consulted when reading Table I where the major (2a) and minor (2b) axes of the scan spots are given both in degrees of geocentric angle and in kilometers. A is the area of the 80 percent power scan spots in square kilometers, and ζ_Δ is the zenith angle of the satellite measured at the scan point.

Table I.

Approximate size of 80 percent power scan spots for various zenith angles of the satellite. Height of satellite, H, equals 750 km.

ζ_Δ	2a		2b		A
deg	deg	km	deg	km	sq km
0	0.81	90	0.81	90	6400
20	0.92	103	0.92	103	8300
30	1.08	120	1.08	120	11300
40	1.42	158	1.11	123	15300
50	1.75	195	1.17	130	19900
60	3.06	340	1.44	160	42800
70	5.91	658	1.84	205	106000

For zenith angles between 0 and 40-45 deg the resolution of the radiometer according to the table must be considered as very good and may be favorably compared with the resolution afforded by the grid of regular synoptic weather stations in well covered areas. For the interpretation of the radiometer measurements as "point values" one should also remember that the sensitivity of the instrument rises rather sharply in the area close to the axis of the beam, which for zenith angles in the interval 0 to 45 deg makes the situation somewhat better than that indicated by the table. For zenith angles greater than 50 deg the resolution deteriorates rapidly; and for zenith angles 60 deg and greater, radiation maps for Channels 2 and 4 are rather unsuited for localization of patterns of ordinary synoptic scale. However, in areas of poor synoptic coverage, and for climatological purposes, radiation measurements for zenith angles in the interval 60 to 70 deg may still give valuable information.

Measurements for zenith angles greater than 75 deg must be discarded for purposes of mapping and synoptic identification, due to the increasing contamination from outer space. For $\zeta_\Delta = 80$ deg, the scan spot (as seen from Figs. 4, 5, 6, and 7) will be cut by the horizon; it will cover approximately 337,000 sq km. The distance from its apex to the horizon will be about 1400 km and the greatest width perpendicular to this line will be about 300 km.

For $\zeta_\Delta = 90$ deg, the radiometer axis will touch the horizon. The scan spot will cover approximately 360,000 sq km of the earth's surface, and have "half axes" equal to 1100 km and 210 km respectively.

The effect of the large scan spots is twofold: first there is the averaging effect over the scan spot area which will tend to smear out the synoptic patterns; secondly, and equally important for the identification of synoptic patterns, there are the distortions which arise from the varying size and orientation of the scan spots over the field. How serious these distortions will turn out depends upon the horizontal variation of temperature, the concentration of water vapor, the height of the upper cloud surface, and the relation of the aforementioned variables to the size and orientation of the scan spots. Some examples will be given in later sections.

Figures 4, 5, 6, and 7 show zenith angles of the satellite measured from the scan points for Orbits 142 and 143, and, in addition, examples of the size and orientation of the scan spots from various parts of the scanned area. Since this is mainly a case with open mode, what we call the initial scan will usually be that part of the scan line that reaches from the first horizon to the scan boundary south of the subpoint track; correspondingly, the complemental scan will be that part of the scan line that reaches from the scan boundary to the second horizon.

From these figures it is obvious that very serious distortions must be expected on the radiation maps produced by either of the two initial scans (Figs. 4 and 6). For the purposes of depicting and localizing patterns of ordinary synoptic scale one will expect these maps to be virtually useless.

The initial scans of Orbit 143 (Fig. 6), especially provide very poor data for the area we are considering. Only a small section in the southwest corner of the map, less than 10 percent of the whole area swept by the initial scans, has zenith angles less than 60 deg. Even the area with zenith angles less than 70 deg is smaller than 20 percent of the whole. One should also notice that within the area of zenith angles less than 70 deg there is a rapid change with location of the orientation of the scan spots. All these factors combine to produce large distortions in the radiation patterns reproduced by the initial scans of Orbit 143.

The initial scans of Orbit 142 (Fig. 4) are slightly better for our purpose since the area with zenith angles smaller than 70 deg is about one-third of the whole area. However,

considerable distortions and dislocations must be expected over most of the area.

For the complemental scans the case is quite different. In Orbit 143 (Fig. 7) the area with zenith angles less than 30 deg has a very good location in relation to the frontal zone and the main cloud systems. Also, zenith angles between 60 and 70 deg cover only a rather small portion of the scanned area which was used in our analysis.

The complemental scans (Fig. 5) of Orbit 142 are also rather satisfactory, if not quite as good as those of Orbit 143. For most of the southeastern half of the area, the complemental scans can be expected to produce radiation maps without too serious distortions and dislocations.

These considerations stress the importance of consulting maps like Figs. 4, 5, 6, and 7 whenever one is confronted with the task of interpreting a map obtained by radiation measurements from satellites. The figures also show the necessity for a separate treatment of the initial and the complemental scans. Model atmospheres and theoretical treatments of radiation transfer problems as a whole are, of necessity, based on the assumption of a horizontally stratified atmosphere. Figures 4, 5, 6, and 7 show that theoretical results should not be uncritically applied to data recorded by satellites of the TIROS III type for zenith angles greater than some 50 deg.

It is to be understood of course that the limits given above depend on the satellite's height, the radiometer's aperture, and the variation in sensitivity across the field of the radiometer. If these parameters are altered, the limits will also have to be changed.

IV. EFFECTIVE BLACK-BODY TEMPERATURES DERIVED FROM CHANNEL II MEASUREMENTS

In Fig. 8 is given the distribution of the effective black-body temperatures, derived from the Channel 2 measurements of Orbit 143 complemental scan. As mentioned in the last section the angular resolution should be quite good for this map. In fact, the area with zenith angles less than 40 deg covers more than half of the total area including most of the major cloud systems connected with the frontal system. In this area, then, most of the details shown in the map should be acceptable without further smoothing of the pattern.

The major features that were mentioned in connection with Fig. 1 show up very well in the radiation temperatures. The cloud system connected with the low in the Great Lakes

region appears in Fig. 8 with three pronounced cold spots of temperatures down to -30C and -50C, respectively. In the U.S. Standard Atmosphere this would correspond to heights of 23,000, 30,000, and 33,000 ft respectively, for the cloud tops. Also the squall line running between the two surface lows is very conspicuous; along its "axis" the temperature varies between -12C and -24C corresponding to heights of 14,000 and 20,000 ft for the upper cloud surface. The orientation of the squall line is parallel to the 300-mb surface wind. The location of the squall line is, on the average, a couple of hundred kilometers northwest of the front on Fig. 1; but this, as mentioned in Section II, does not necessarily mean that there is an inconsistency between the two maps apart from the difference in the time of observation. In the area with clear or relatively cloud-free conditions north of the squall line, the radiation map shows a conspicuous warm tongue of air parallel to the squall line with temperatures in the interval 6C to 8C.

It is also interesting to see how well topographic features show up in the radiation pattern for areas where we have reason to assume there are few or no clouds. Starting near the scan boundary in the south and close to the 105 W-meridian, there are several closed isotherms with temperatures between 0C and -2C, running in a northwesterly direction and obviously connected with the Continental Divide. As a contrast we find in the Painted Desert area temperatures from 8C to 12C, and in the northern end of the Gulf of California and in the Imperial Valley temperatures slightly above 20C. It should be kept in mind, however, that differences in effective black-body temperatures between lowlands and mountains are very dependent upon the hour of the day. During daylight the picture may be entirely different from the one presented here.

A comparison of Fig. 8 with Figs. 1, 2, and 3 shows clearly that the radiation pattern derived from Channel 2 measurements can give useful synoptic information even if satellite pictures are lacking, provided some care is taken in the interpretation of the radiation maps. There are, certainly, conditions where some confusion will arise: snow covered areas with strong ground inversions may be difficult to distinguish from areas with a uniform and not too high cloud cover; areas with broken clouds may be difficult to separate from mountain ranges. In many such cases a certain knowledge of the general synoptic situation, derived from other sources, will solve the difficulty. Especially would one like to think that the Channel 2 measurements might be a valuable supplementary synoptic tool over tropical oceans despite their traditionally poor synoptic coverage.

Thus far we have been concerned mainly with radiation in more or less relative terms. One of the uses originally intended for Channel 2 was to make inferences about the temperatures of the radiating surfaces. To obtain these from the Channel 2 measurements, certain corrections will have to be added to the values on our map. Wark, Yamamoto, and Lienesch (1962 and 1963) have given a method for estimating this correction. Some uncertainty will still exist due to the amount and vertical distribution of water vapor and ozone in the intervening atmosphere which can in many cases only be roughly estimated. In addition there are the little known effects of emission and scattering by aerosols. The temperatures thus arrived at should be the surface radiation temperatures, which will sometimes differ considerably from the air (shelter) temperatures, usually the only ones available for comparison.

For the highest cloud tops with black-body temperatures between -30C and -50C the true temperatures according to Wark, Yamamoto, and Lienesch, should be only 1C to 3C higher than our values. For most of the cloud-free areas we have the additional complication that these in Orbit 143 occur in mountainous country. Therefore, the temperatures reported by the synoptic stations may vary widely, depending upon their locations. There are, however, a few areas where a comparison can be reasonably undertaken. Along the lower part of the Colorado River the synoptic stations at 0900 GCT report temperatures between 28C and 32C, while the Channel 2 black-body temperatures are in the interval between 18C to 20C. Also in the Dakota-Minnesota area we have two regions with apparently cloud-free conditions. In one of these regions the air (shelter) temperatures at 0900 GCT are reported as about 10C, while the Channel 2 temperatures are 1C to 4C. In the other region the air temperature is reported at about 16C, while the Channel 2 temperatures are 6C to 8C. All these differences are slightly larger than one would expect according to Fig. 16 in the quoted work by Wark, Yamamoto, and Lienesch. On the whole, however, the Channel 2 temperatures we have obtained are acceptable when one keeps in mind that it is the surface radiative temperature and not the air (shelter) temperature that, in the main, will determine the energy flux in Channel 2.

As an example of the effects of altitude we turn to the Colorado Rockies, also, according to synoptic evidence, a cloud-free area. The Channel 2 temperatures between 0C and -2C correspond quite well to the standard atmosphere temperatures given for these

altitudes (9,000 to 13,000 ft). The given examples may be taken as an indication that the final corrections we have applied to the Channel 2 measurements lead to results that cannot be very far from the true, effective, black-body temperatures.

Turning now to Orbit 142 complemental scans, Fig. 9, we notice a general agreement in the scanned areas common to both maps. This holds, however, only as far as the patterns are concerned, and even for these not in all details. If we compare absolute values, the agreement is no longer as good. However, most of the differences can be explained quite easily, at least in a qualitative sense, as being due to differences in optical path length combined with the averaging effects of large scan spots. We shall give some examples, and start with the warm tongue of air immediately north of the squall line.

In the narrow southwest portion of the tongue, the temperatures in Fig. 9 rise to -6C or -5C. The zenith angles are, for this case (Fig. 5), about 55 deg with the major axis orientated perpendicular to the strong gradients on both sides of the tongue. In Orbit 143 (Fig. 8) the temperatures in the same area were as high as 6C and the zenith angles only about 25 deg. Compare now the two pictures, presented, of the squall line. For Orbit 142 (zenith angles 50 to 55 deg) we find temperatures -16C to -20C in the cold spots in the southwest. For Orbit 143 (zenith angles 20 to 30 deg) the temperatures in the corresponding area are -20C to -24C. Finally, in Orbit 142 the large central cloud mass northwest of the warm tongue has temperatures down to -40C; in Orbit 143 in the same area we find -36C. To get a clearer picture we have put these temperatures together below:

	Central Cloud Mass	Warm Tongue	Squall Line
R/O 142	-40C	-6C	-18C
R/O 143	-36C	+6C	-22C

The time interval between the two flights is, as mentioned earlier, about 100 minutes, and some development has undoubtedly taken place in the system during this period. When looking at the sequences of numbers presented above, however, one cannot escape the conclusion that the main cause for the smaller contrasts in the picture presented by Orbit 142 as compared with Orbit 143 must be the averaging effect due to the size and orientation of the scan spots in Orbit 142. The case is perhaps an extreme one, but still has considerable interest for the following reason: it has been proposed on several occasions to use the effect

of limb darkening, as shown by satellite measurements at varying zenith angles, in order to obtain information about the amount and distribution of water vapor in the intervening atmosphere. The example above shows the danger of an uncritical application of a theoretical result to this problem. A calculation of limb darkening which takes into account the effects of increasing scan spots for large zenith angles has been made by Larsen, Fujita, and Fletcher (1963).

Another example of the same effect is given by the isolated cloud information in Orbit 143 at 42N, 102W, an area with a zenith angle of about 10 deg. In Fig. 9, this structure is hardly recognizable. It might be argued that dynamical effects alone would be able to produce this result. A closer inspection of the pattern in Fig. 9, however indicates that the structure still exists but has been merged with the huge central cloud mass as a result of the size and orientation of the scan spots in this area.

Finally we will compare Figs. 8 and 9 at the northern end of the Gulf of California. In Fig. 8 we find a warm tongue with temperatures in the range 18C to 21C. Here the zenith angles for the scans range from 20 to 30 deg. In Fig. 9 there is also a warm tongue but the temperatures are only 10C to 14C. According to Fig. 5 the zenith angles were for these scans close to 70 deg with the major axis orientated W-E. It seems that limb darkening in the proper sense is mainly responsible for the lower temperatures displayed by Fig. 9.

These are only a few examples of the caution that must be exercised when Channel 2 measurements are being used for mapping synoptic structures. Essentially it is a question of the scale of the phenomenon one has in mind. For the study of structures on a synoptic scale, and above all, for study of mesoscale structures, maps like Figs. 4, 5, 6, and 7 should always be at hand as an aid for the interpretation.

Obviously, as can be seen from Fig. 5, the "truest" part of the map in Fig. 9 is the area stretching northeast from the Gulf of Mexico. In the northern part of the State of Mississippi there is, apparently, a cloud-free area where the synoptic stations report temperatures of 23C to 25C at 0900 GCT. The Channel 2 temperatures at zenith angles about 20 deg are 16C to 20C. Again, as in the case of Fig. 8, the differences seem acceptable.

V. EFFECTIVE BLACK-BODY TEMPERATURES DERIVED FROM CHANNEL 4 MEASUREMENTS.

On the maps we have drawn on the basis of the Channel 4 measurements we shall only make some brief comments. In Fig. 10 we have presented the Channel 4 effective black-body temperatures produced by Orbit 143 complemental scans. Between this map and the Channel 2 map (Fig. 8) there is of course, a great similarity in the general patterns in spite of the differences in temperature values. In the warm, cloud-free area over the northern part of the Gulf of California and adjacent land areas, the Channel 4 temperatures are, in places, as much as 24C to 26C lower than the Channel 2 temperatures. In the coldest spots in the great cloud mass in the Kansas-Oklahoma area the differences amount to some 4C to 8C. Along the squall line we find differences of 6C to 12C. There is, therefore, a quite systematic reduction in the differences between Channel 2 and Channel 4 temperatures with decreasing Channel 2 temperatures. The effect of this is, of course, to make the contrasts between hot and cold spots much smaller in Fig. 10 than in Fig. 8.

For the cold spots in the very high cloud masses of the Great Lakes region one should expect the differences between Channel 2 and Channel 4 to be very small due to the great height of the upper cloud surface there. This is also true for the cold spot at the northern end of Lake Michigan where both maps show temperatures of about -50C. For the cold area over the western end of Lake Superior the situation is apparently a bit different. In the Channel 2 temperatures (Fig. 8), we find one cold area of an elongated shape and the lowest temperature equal to -44C. On the Channel 4 map (Fig. 10), we find two cold centers with temperatures -54C and -60C, respectively. As the zenith angle in this area is rather small (15 to 30 deg), differences as large as these are rather unlikely. The most probable explanation is that the values in Fig. 10 are too low, either due to "noise" or to errors committed in the reading of the Brush Record Tape. If we discard these Channel 4 values, we will also make the values for the total infrared fluxes more reasonable from a theoretical point of view.

The next figure (11) has been included mainly for the sake of illustrating the effects of very large scan spots. Part of the scanned area (for zenith angles less than 70 deg) has been used to compute the total infrared fluxes in the next section. As will be seen there is rather little similarity between Figs. 10 and 11, although the time differences in the scanning

of one particular location is just a matter of a few minutes. The northern half of the scanned area of Fig. 11 is dominated by the effect of contamination from outer space. But even in most of the places where this effect has been avoided, the large scan spots in Fig. 11 produce dislocations and distortions of such a magnitude that the main patterns shown in Fig. 10 are difficult to recognize except in their broadest outlines.

In Fig. 12 we have the Channel 4 effective black-body temperatures from Orbit 142 complemental scans. Again there is a great similarity to Fig. 9, in the same sense as was the case for the other pair, Figs. 8 and 10. Finally, in Fig. 13 we have the Channel 4 effective black-body temperatures from the initial scans of Orbit 142. This like Fig. 11 is again an illustration of the effects of large zenith angles. In the northeastern part of the map, the effect of contamination from outer space is rather conspicuous. In those parts of the map where the zenith angles are less than 70 deg, several of the large scale features are still recognizable; but dislocations and distortions make a point to point comparison with Fig. 12 rather futile.

VI. COMPUTATION OF THE TOTAL OUTGOING INFRARED FLUX

The method we employed for the computation of the total infrared flux was one proposed by Wark, Yamamoto, and Lienesch (1962, 1963). In its original form the method was not very well suited for work with maps. Therefore a series of tables and graphs was prepared which enabled us to find the values of the total infrared flux when the zenith angles and the effective black-body temperatures derived from TIROS III Channel 4 measurements are known. A short description of the procedure will be given.

For the total infrared specific intensity $I(\zeta_\Delta)$, at zenith angle ζ_Δ, Wark, Yamamoto, and Lienesch, studying the transfer of radiation through model atmospheres, found the empirical relation:

$$I(\zeta_\Delta) = g'T_B^3 + f'T_B^2 + e'T_B + d' \qquad (1)$$

where T_B is effective black-body temperature derived from TIROS III, Channel 4 measurements. The parameters g', f', e' and d' should in principle depend upon the zenith angle. However, this variation was found to be so small that, for all practical purposes, it could be neglected. In Eq (1) these parameters are, therefore, given constants. Incidentally,

the values given by Wark, Yamamoto, and Lienesch are such that $I(\zeta_\Delta)$ given by Eq(1) is not total specific intensity proper, but specific intensity multiplied by π . From Eq (1) the following table was computed:

Table II

Total specific intensity (multiplied by π) as a function of effective black-body temperatures.

t	$I(\zeta_\Delta)$	t	$I(\zeta_\Delta)$
-90C	0.108	-20C	0.322
-80C	0.126	-10C	0.373
-70C	0.148	0C	0.430
-60C	0.174	10C	0.493
-50C	0.203	20C	0.564
-40C	0.238	30C	0.642
-30C	0.277		

The units for $I(\zeta_\Delta)$ are langleys per minute.

From Table II a graph was prepared that enabled us to read off $I(\zeta_\Delta)$ for intermediate temperatures with an error of 1 to 2 units in the third decimal.

Next comes the question of the limb darkening. From their model studies Wark, Yamamoto, and Lienesch deduced the following empirical relation between the total intensity at zenith angle zero, $I(0)$, and $I(\zeta_\Delta)$:

$$I(\zeta_\Delta) = I(0)\left[1 + (\alpha+\beta I(0))\cdot(a\zeta_\Delta + b\zeta_\Delta^2 + c\zeta_\Delta^3)\right] \qquad (2)$$

in which α, β, a, b, c are constants determined in order to give best fit.

As an example the relation for $\zeta_\Delta = 40$ deg is explicitly given:

$$I(40) = 1.0166\, I(0) - 0.0864\, I(0)^2 \qquad (2a)$$

Inserting values of $I(0)$ into equation (2a) and the corresponding ones for other zenith angles, the corresponding values for $I(\zeta_\Delta)$ were obtained. Using then the graph prepared from Eq (1) and Table II, corresponding values of $I(0)$ and Channel 4 effective black-body

temperatures were obtained for various zenith angles. Again as an example, Table III gives this relationship when $\zeta_\Delta = 40$ deg:

Table III

$I(0)$ as a function of temperature at zenith angle $\zeta_\Delta = 40$ deg.

t(40)	I(0)	t(40)	I(0)
-93.9C	0.10	-6.5C	0.40
-68.7C	0.15	1.6C	0.45
-51.2C	0.20	9.2C	0.50
-37.3C	0.25	15.8C	0.55
-25.6C	0.30	22.0C	0.60
-15.5C	0.35		

Assuming a horizontally stratified atmosphere, the total infrared flux escaping from the top of the atmosphere is expressed by

$$F = 2\pi \int_0^{\pi/2} I(\zeta_\Delta) \sin\zeta_\Delta \cos\zeta_\Delta \, d\zeta_\Delta .$$

With $I(\zeta_\Delta)$ given by (2) Wark, Yamamoto, and Lienesch obtain the following formula:

$$F = I(0)\left[A + CI(0)\right], \qquad (3)$$

where the values of the constants A and C are determined by the constants in Eq (2). Inserting now values of $I(0)$ in Eq (3), the corresponding values of F are found. Using, then, Table III and similar tables for other zenith angles, values of F, as a function of the zenith angle and the effective black-body temperature, are obtained.

Table IV. gives examples of corresponding values of F and effective black-body temperatures at zenith angles ranging from 0 to 70 deg. From Table IV and other similar tables a graph was prepared (Fig. 14). It was now easy to convert effective black-body temperatures obtained from Channel 4 measurements at various zenith angles to total infrared flux; interpolations for intermediate angles were readily performed. Zenith angles larger than 70 deg were not included due to the effects of contamination from outer space.

Table IV

Total infrared flux, F (langleys per minute), and a function of effective black-body temperature from Channel 4 measurements at various zenith angles.

F	t(0)	t(10)	t(20)	t(30)	t(40)	t(50)	t(60)	t(70)
0.102	-94.7	-94.7	-94.7	-94.7	-93.9	-93.9	-93.3	-92.0
0.151	-69.1	-69.1	-69.1	-69.1	-68.7	-68.7	-68.4	-68.0
0.200	-51.2	-51.2	-51.2	-51.2	-51.2	-51.2	-51.2	-51.5
0.248	-37.0	-37.0	-37.0	-37.3	-37.3	-37.5	-38.0	-38.5
0.294	-25.0	-25.0	-25.2	-25.2	-25.6	-26.1	-26.8	-27.9
0.340	-14.5	-14.6	-14.6	-15.0	-15.5	-16.0	-17.3	-18.9
0.386	- 5.2	- 5.4	- 5.5	- 5.9	- 6.5	- 7.5	- 9.0	-11.2
0.430	3.3	3.2	2.8	2.5	1.6	0.2	- 1.5	- 4.7
0.473	11.1	10.8	10.5	10.0	9.2	7.6	5.1	1.3
0.516	18.2	17.9	17.5	16.9	15.8	14.0	11.1	6.6
0.558	24.7	23.3	23.9	23.3	22.0	19.9	16.5	11.2
0.598						24.7	21.5	15.4

VII. MAPS OF OUTGOING TOTAL INFRARED FLUXES

In Fig. 15 we have presented the total infrared fluxes derived from the complemental scans of Orbit 143. Only those parts of the scans where the zenith angles are less than 70 deg have been utilized. A main characteristic of Fig. 15 is the uniformity of the values in the western areas. Over a large portion of the scanned area one finds fluxes between 0.38 and 0.44 ly per minute. A similar uniformity of outgoing total infrared fluxes is also found in theoretical calculations of this quantity for cloudless areas, since the effect of higher air temperature is more or less neutralized by a higher content of water vapor.

According to theoretical estimates by Yamamoto, (1952) the values of outgoing total infrared fluxes should range from 0.2 to 0.4 ly per minute; for most of the area our values

are also contained within these limits. There are, however, areas for which this is not true.

From the very high clouds in the area northwest of Lake Superior, the outgoing flux amounts only to some 0.17 ly per minute. However, as explained in Section V, there is reason to believe that the low temperatures recorded by Channel 4 in this region are fictitious, and this would raise the flux values above Yamamoto's critical lower limit. The values between 0.40 and 0.44 ly per minute in the west are more difficult to explain if we adopt, as correct, Yamamoto's estimates. In this connection it should be kept in mind that we are studying a night case, and that during daylight the recorded maximum fluxes would be still greater because the soil temperatures are considerably higher in our case. Another circumstance that should be noted is that these high flux values are found in areas where the zenith angles vary from 15 to 70 deg, and there is, apparently, no significant variation with changes in the zenith angle.

Here the question about the limb darkening law adopted by Wark, Yamamoto and Lienesch must be considered. As pointed out by these authors, the effect of underestimating the limb darkening will depend upon the zenith angles at which the measurements are made. If the outgoing radiation has been measured by the satellite at a small zenith angle, the actual flux will, on the assumption of a horizontally stratified atmosphere, be smaller than the flux computed by their method. If, on the other hand, the measurements are taken at a large zenith angle, the actual flux will, again assuming a horizontally stratified atmosphere, be greater than the computed value. If the limb darkening in our computational scheme is exaggerated, the discrepancies for small and large zenith angles, respectively, will be the reverse of those quoted above. The circumstance that the varying zenith angles apparently have no effect on the great fluxes in the western area and may be taken as an indication that the limb darkening law adopted by Wark, Yamamoto, and Lienesch is approximately correct for the conditions prevailing in this area.

As will be seen from Fig. 16, the fluxes based on the complemental scans of Orbit 142, have still larger maximum value, $F = 0.46$ ly per minute for zenith angles between 65 and 70 deg. According to the authors themselves, it is rather improbable that they exaggerated the limb darkening. These excessive values therefore, represent a problem.

One explanation, of course, would be that Yamamoto's upper limit is too low. To test this possibility we made some tentative computations on atmospheric transmissivity.

On one hand we took the data and the technique proposed by Wark, Yamamoto, and Lienesch. On the other hand we took the data and the computational procedure proposed by Elsasser and Culbertson (1960). Transmissivities in selected wave lengths of the water vapor spectrum were computed for the atmospheric model designated as No. 37 in the paper by Wark, Yamamoto, and Lienesch. It turned out that the transmissivity values we obtained for these wave lengths, by means of Elsasser's and Culbertson's procedure, were consistently lower than those obtained by the method of Wark, Yamamoto, and Lienesch. A cursory inspection seemed to confirm that this would also be the case for most other regions of the water vapor spectrum. Although the test is not entirely conclusive, it indicates that Elsasser's and Culbertson's absorption data will probably lead to still lower values than Yamamoto's for the outgoing radiation.

Another, and more probable, explanation may be found in the final corrections we applied to the Channel 4 measurements for Orbits 142 and 143. According to the personal communication received from W. Bandeen and referred to in the introduction, this correction should add 10C to values in the -20C to 0C interval obtained from the original calibration. It is quite possible that this correction overcompensates for the instrumental degradation processes they were supposed to eliminate in the mentioned interval.

Total outgoing infrared flux is a quantity of such significance that it would be very desirable to have means for testing the methods by which it has been computed. Obviously a value which is based on a single measurement at a certain zenith angle can be only interpreted as a more or less probable value; hence local deviations from true values may be considerable. The most one can hope to obtain is fairly accurate mean values for areas large enough to cover various conditions of zenith angles and atmospheric structure. The separation of the radiation data into initial and complemental scans gives us two sets of data from partly overlapping regions, separated in time by only a few minutes. Due to the distortions and dislocations resulting from the different sizes and locations of the scan spots, it would be rather futile to look for any significant agreement when comparing "point values" of the flux. We have, therefore, concentrated on mean values for areas so large that the disturbing influences from outside the boundary should be tolerable. We have applied the test to both our orbits.

In the case of Orbit 143 there was, as will be seen from Figs. 6 and 7, only a rather small area located around an average latitude of 33N where both the initial and the comple-

mental scans had zenith angles less than 70 deg. For purposes of integration, this area was divided into 86 "quadrilaterals", each formed by the intersections of one-degree meridians and latitude circles. Incidentally, an area in the neighborhood of 30N and consisting of 100 quadrilaterals, as defined above, will cover about 0.2 percent of the total area of the earth.

In the case of Orbit 142 there was a somewhat larger common area, located between 25N and 35N, where the zenith angles in both initial and complemental scans were less than 70 deg (Figs. 4 and 5). For purposes of integration this was divided by the meridian 99W in two, approximately equal areas: a western area consisting of 122 quadrilaterals, and an eastern area consisting of 134 quadrilaterals. The mean values of the flux are given for each area in Table V.

Table V

Mean values for outgoing total infrared flux.

Orbit 142

	Initial Scans	Complemental Scans
(W. area)	0.349	0.328
(E. area)	0.369	0.366
(W. & E. area)	0.359	0.348
	Orbit 143	
	0.370	0.371

The agreement must be considered excellent except, perhaps, for the western area Orbit 142 where it may be said to be at least satisfactory. The standard deviations of the quadrilateral means from the overall means have also been compared for the various areas and are listed in Table VI.

Table VI

Standard deviations of quadrilateral means of fluxes from overall means.

Orbit 142

	Initial Scans	Complemental Scans
(W. area)	0.036	0.055
(E. area)	0.033	0.041
(W. & E. area)	0.036	0.052
Orbit 143		
	0.055	0.052

The extreme values of the quadrilateral means are shown in Table VII:

Table VII

Maximum and minimum values of quadrilateral means of outgoing total infrared flux.

Orbit 142

	Initial Scans		Complemental Scans	
	F(min)	F(max)	F(min)	F(max)
(W. area)	0.260	0.410	0.190	0.440
(E. area)	0.270	0.425	0.215	0.420
Orbit 143				
	0.210	0.425	0.230	0.430

One should expect a larger range of values on the whole in the complemental scans than in the initial scans, since the scan spots are smaller in the former case. This is also the case for Orbit 142. That this will not always be true can be due to disturbing influences from the regions beyond the line, $\zeta_\Delta = 70$ deg. Also, maximum and minimum values are rather sensitive to noise. As Tables VI and VII show, the conditions vary considerably within each of the areas we have tested; this may account for the agreement we have obtained in the mean values since the errors in the individual values will then tend to cancel out.

For our case, the method of Wark, Yamamoto, and Lienesch gives reasonable and consistent mean values of outgoing total infrared flux for areas of the size we have considered. It seems that this method can be applied with some confidence to get mean flux values for cases and areas where the zenith angles are so large that the identification and location of specific features as they appear on ordinary synoptic maps, become of doubtful value. However, more tests for other latitudes and different meteorological conditions are needed before the practical value and the limitations of the method can be ascertained.

REFERENCES

Elsasser, Walter M. and Margaret F. Culbertson, 1960: Atmospheric Radiation Tables. Meteorological Monographs, Vol. 4, No. 23. American Meteorological Society.

Fujita, T., 1963a: Outline of a Theory and Examples for a Precise Analysis of Satellite Radiation Data. Mesometeorology Research Paper No. 15, University of Chicago.

-----, 1963b: A technique for Precise Analysis of Satellite Photographs. Mesometeorology Research Paper No. 17, University of Chicago.

Larsen, S.H.H., T. Fujita, and W.L. Fletcher, 1963: Evaluation of Limb Darkening from TIROS III Radiation Data. Mesometeorology Research Paper No. 18, University of Chicago.

Staff Members, Aeronomy and Meteorology Division, NASA, Goddard Space Flight Center, Greenbelt, Maryland: The Attitude World Map of TIROS III, July, 1961.

Staff Members, Aeronomy and Meteorology Division, NASA and Meteorological Satellite Laboratory, Goddard Space Flight Center, Greenbelt, Maryland: TIROS III Radiation Data User's Manual, August, 1962.

Wark, D.Q., G. Yamamoto, and J. Lienesch, 1962: Infrared Flux and Surface Temperature Determination from TIROS Radiometer Measurements. U.S. Weather Bureau, Meteorological Satellite Laboratory, Report No. 10, with Supplement, April, 1963.

Yamamoto, G., 1952: On a Radiation Chart. The Science Reports of the Tohoku University, Series 5, Vol. 4, pp. 9-23.

FIGURES

(Cross index of page references)

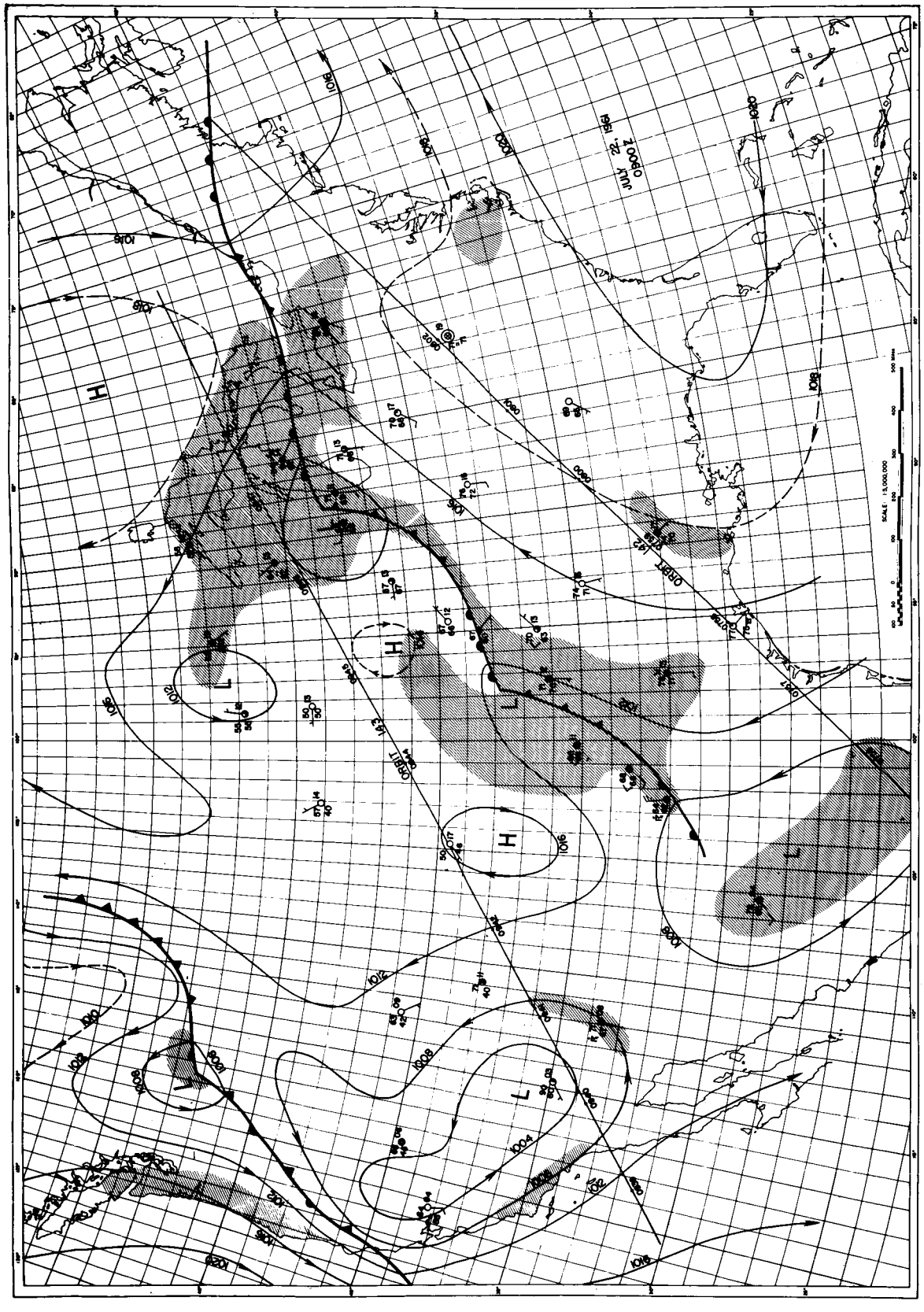

Fig. 1 Surface Weather Map, 22 July 1961, 0900 GCT (U.S. Weather Bureau)

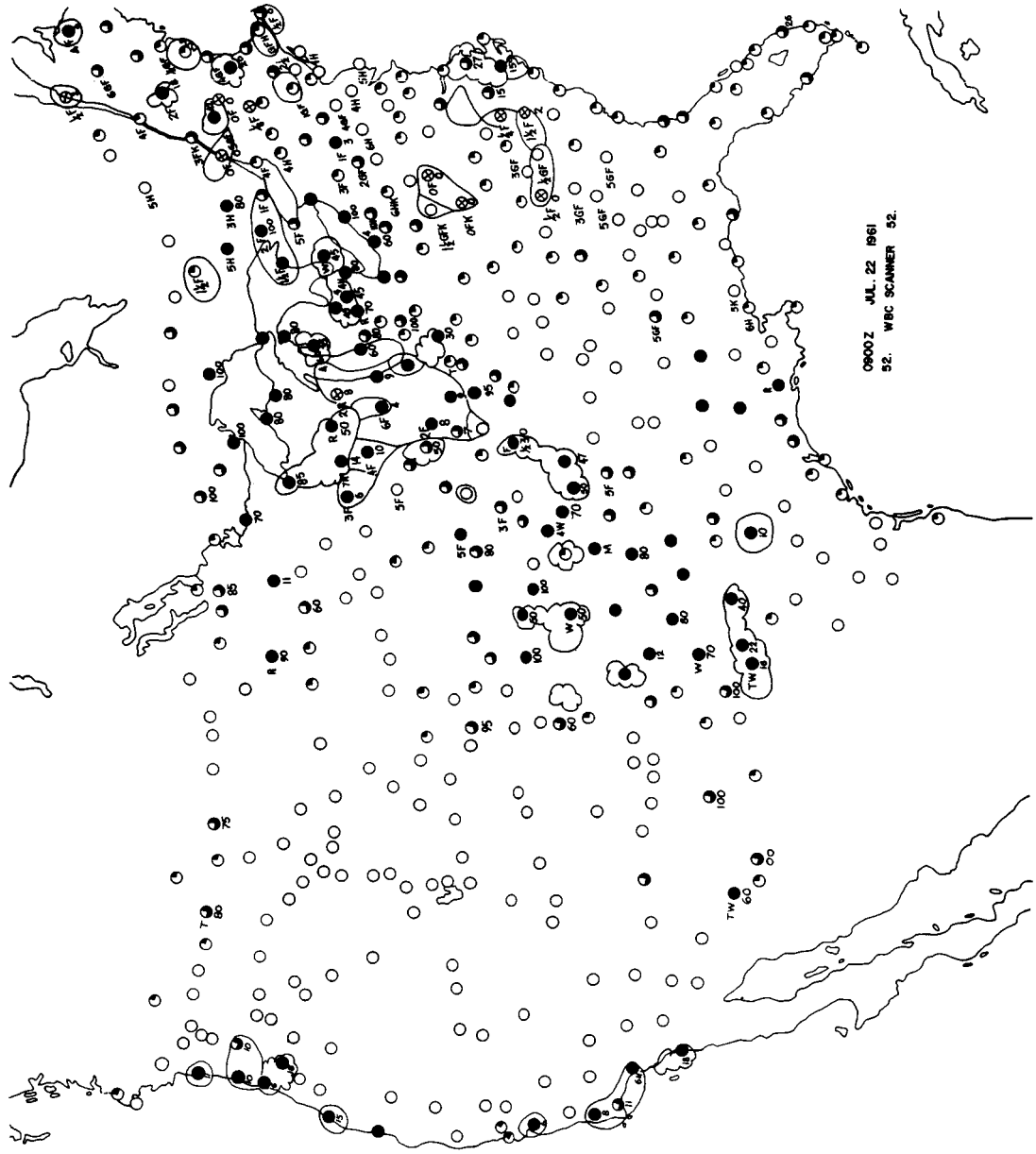

Fig. 2 Distribution of clouds, 22 July 1961, 0900 GCT (U. S. Weather Bureau)

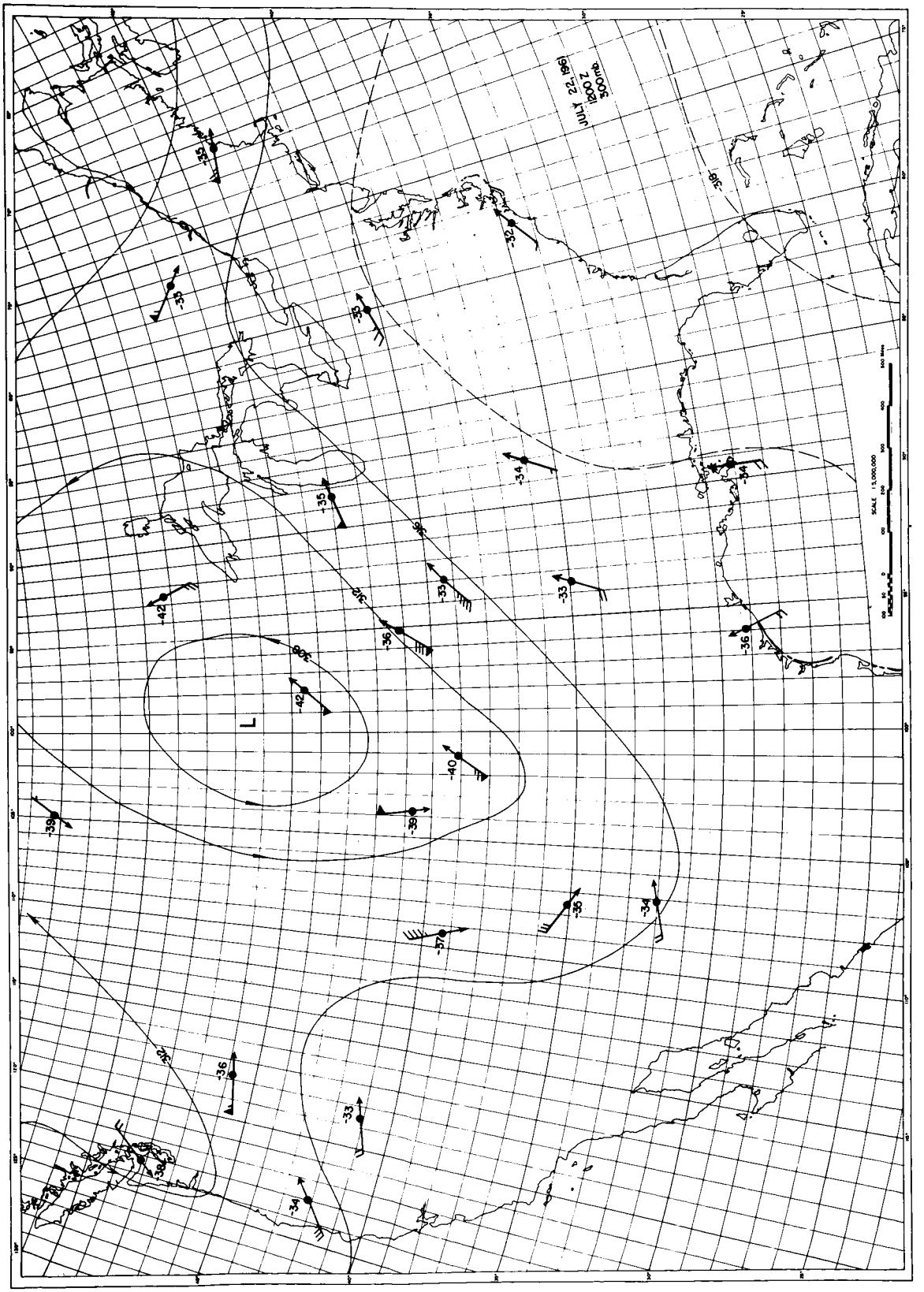

Fig. 3 300-millibar surface map, 22 July 1961, 1200 GCT (U.S. Weather Bureau)

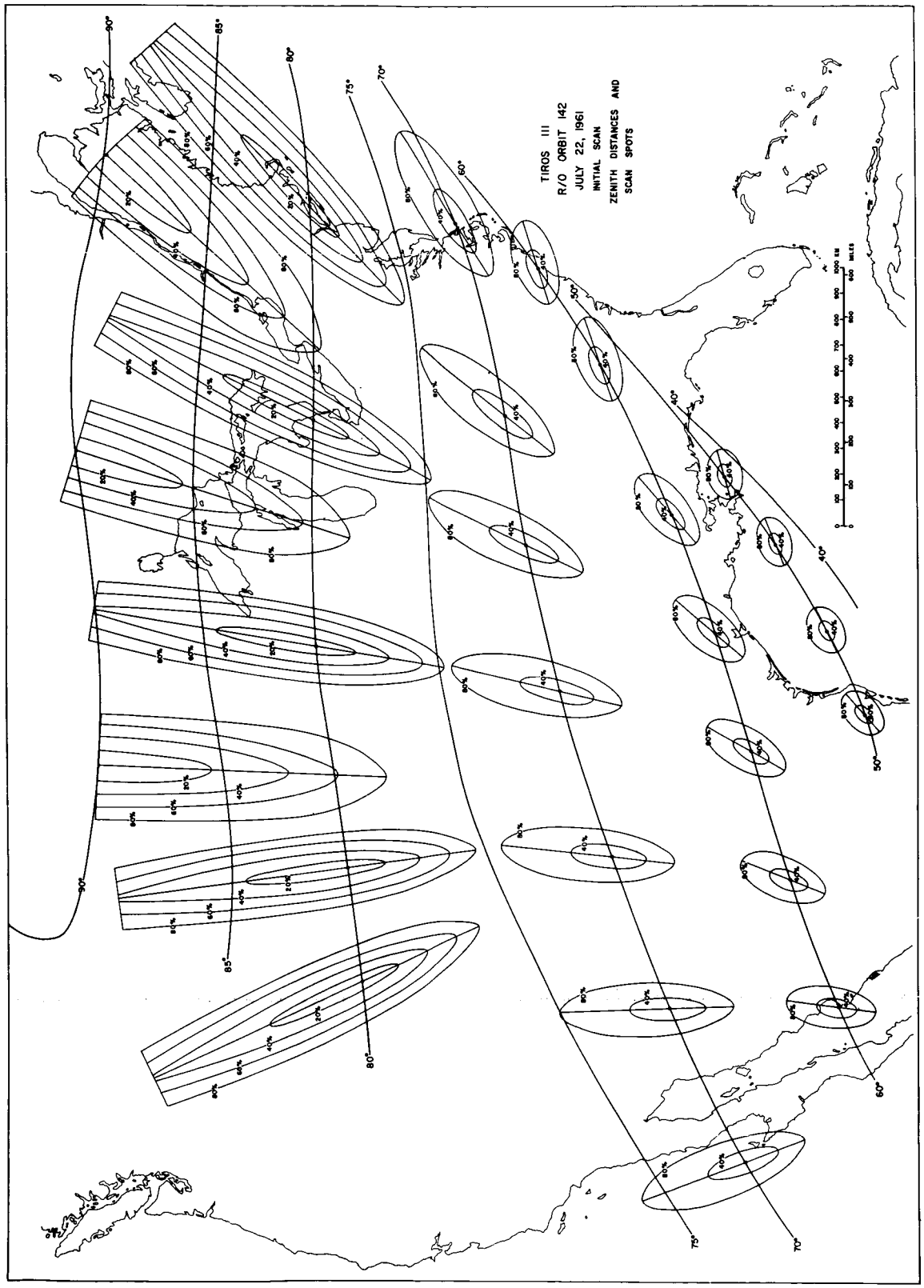

Fig. 4 Orbit 142 initial scans. Scan spots and zenith angles of satellite, measured from scan points.

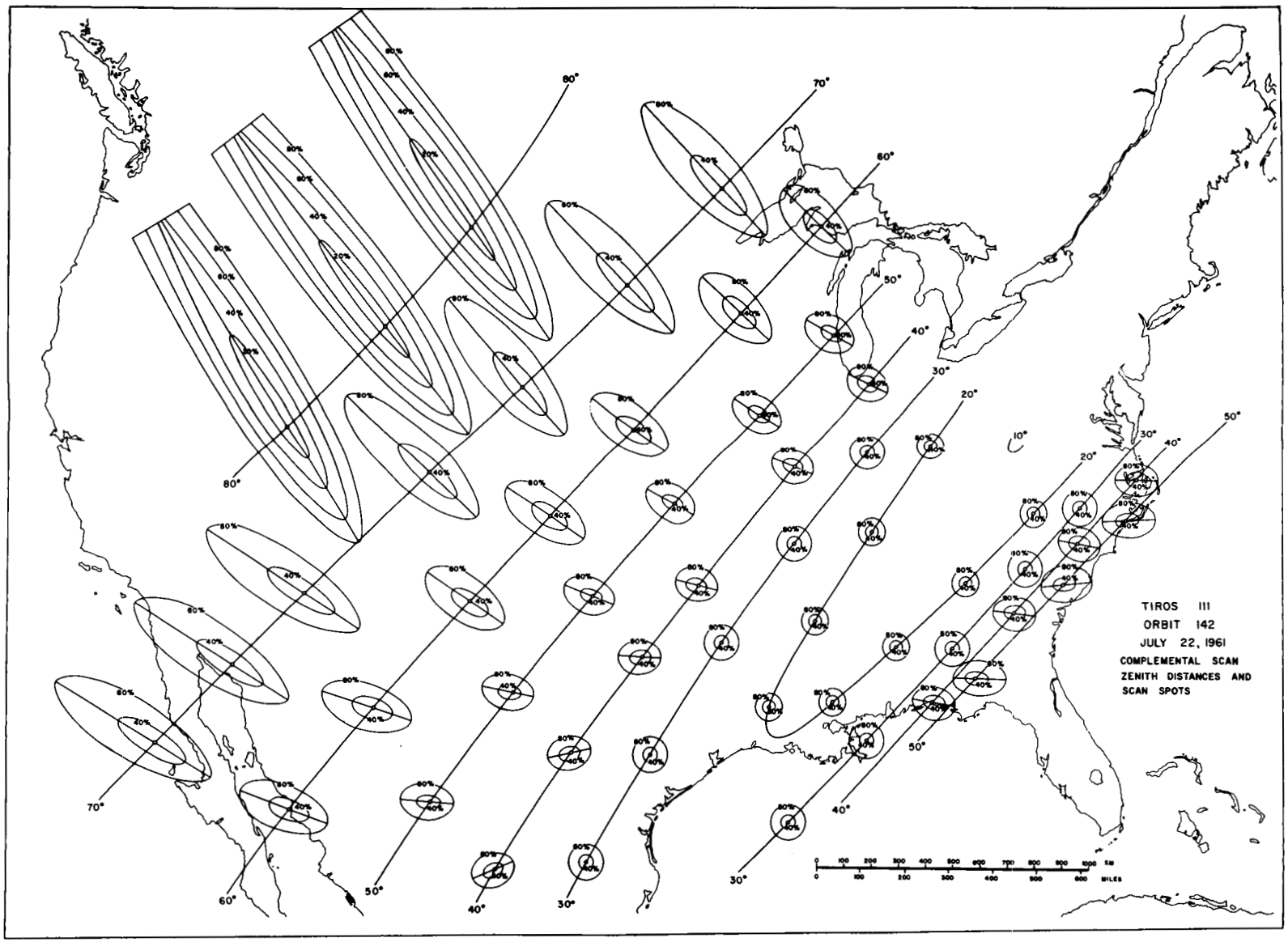

Fig. 5 Orbit 142 complemental scans. Scan spots and zenith angles of satellite, measured from scan points.

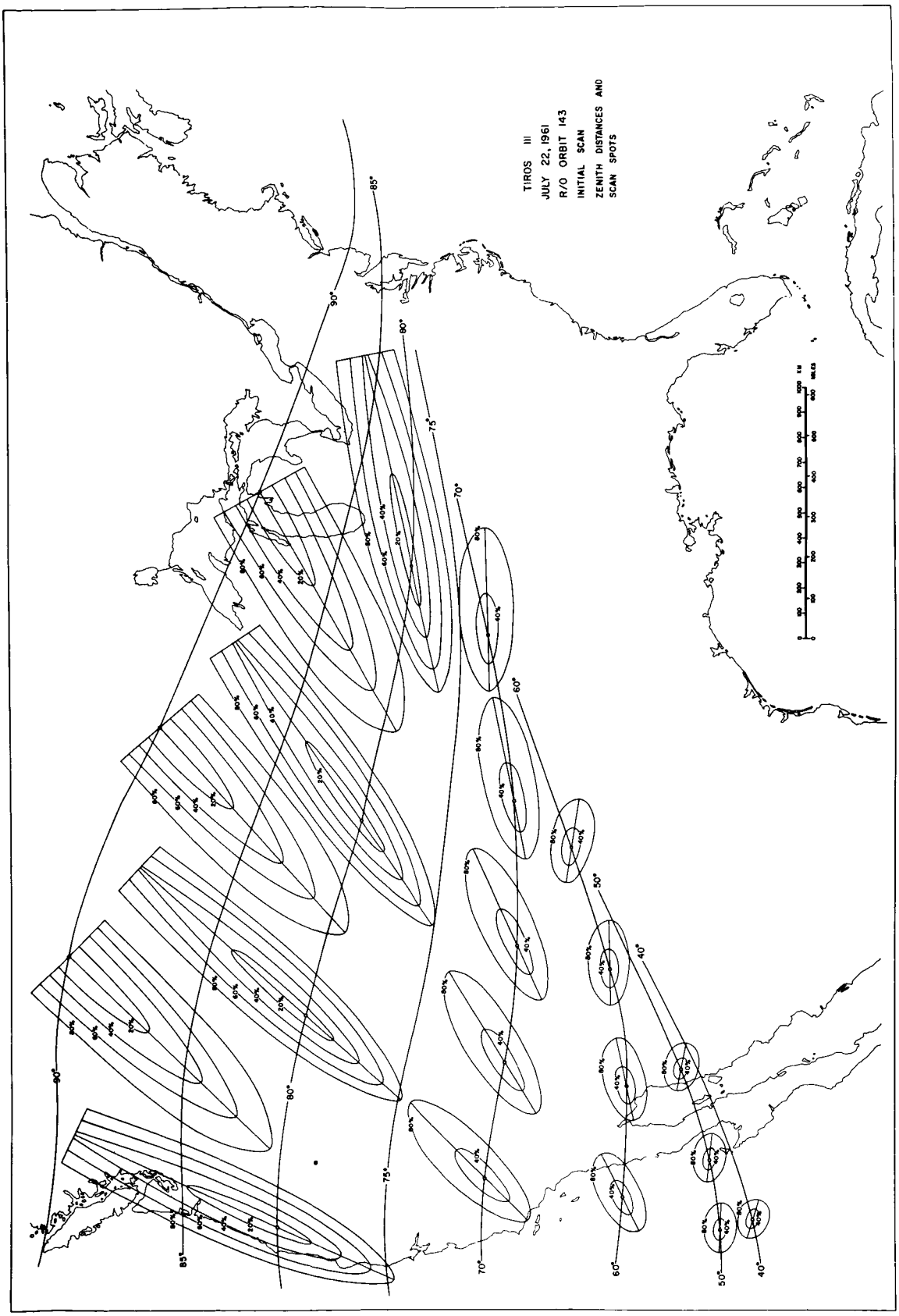

Fig. 6 Orbit 143 initial scans. Scan spots and zenith angles of satellite, measured from scan points.

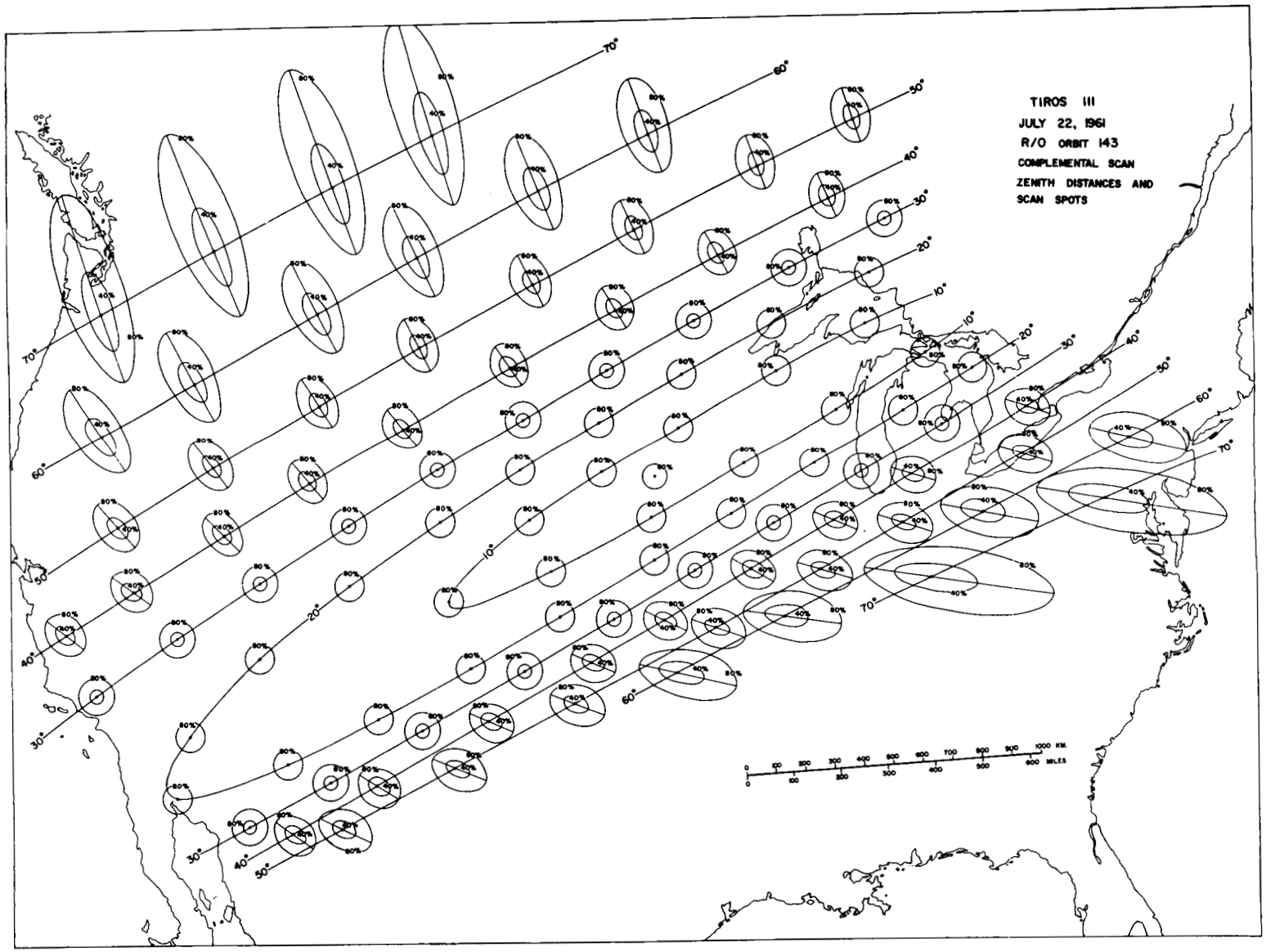

Fig. 7 Orbit 143 complemental scans. Scan spots and zenith angles of satellite, measured from scan points.

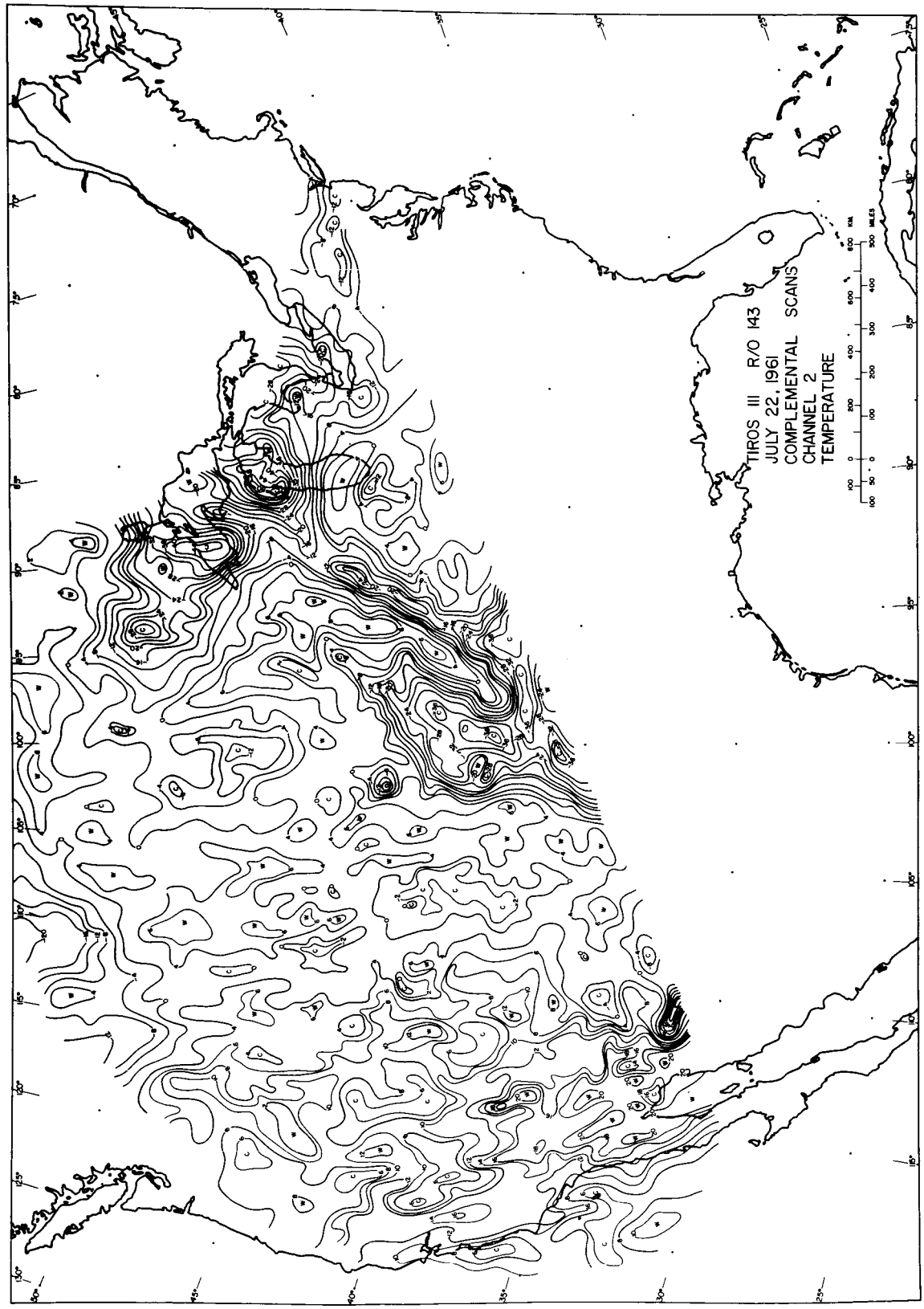

Fig. 8 Effective black-body temperatures. Orbit 143, Channel 2 complemental scans.

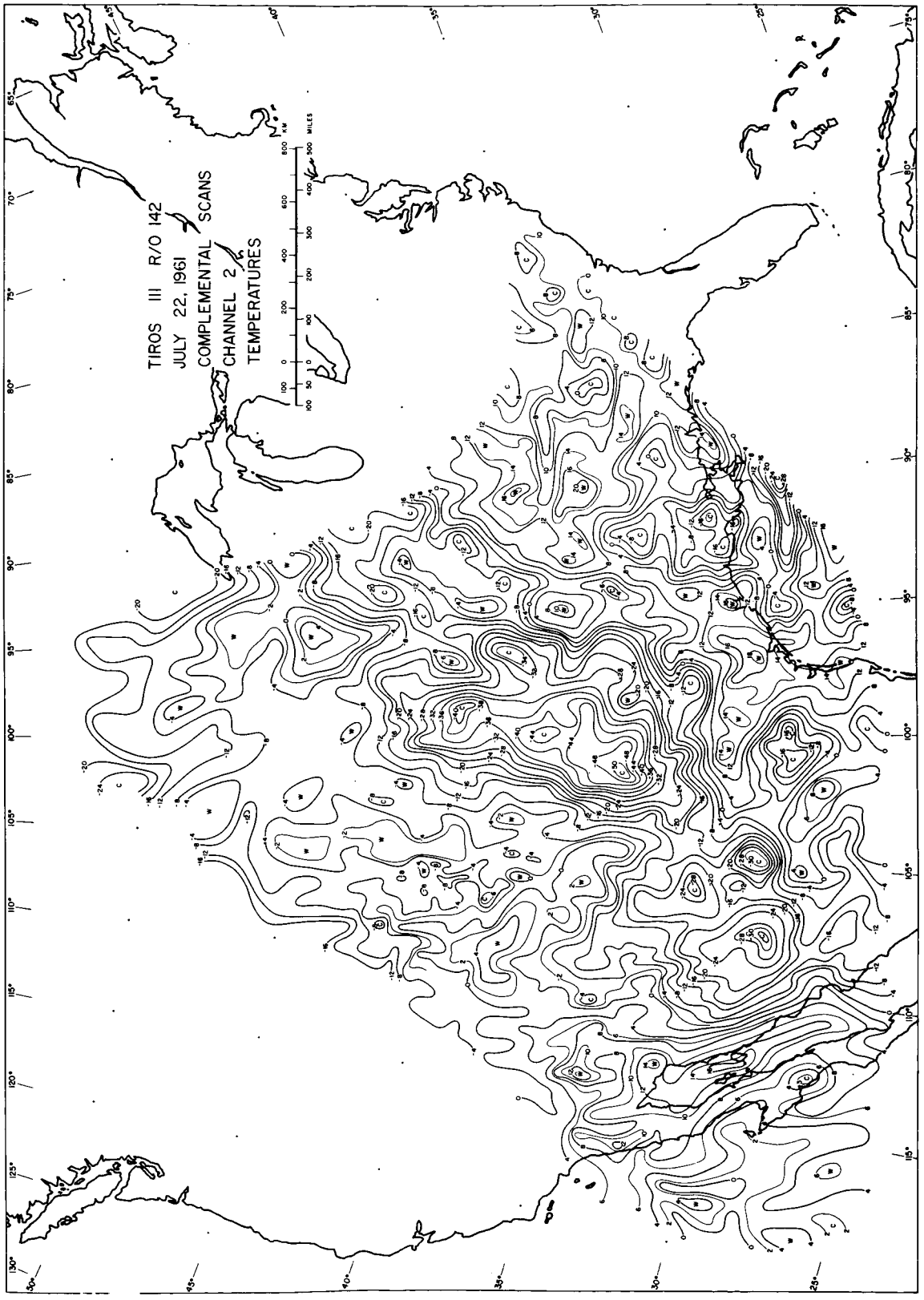

Fig. 9 Effective black-body temperatures. Orbit 142, Channel 2 complemental scans.

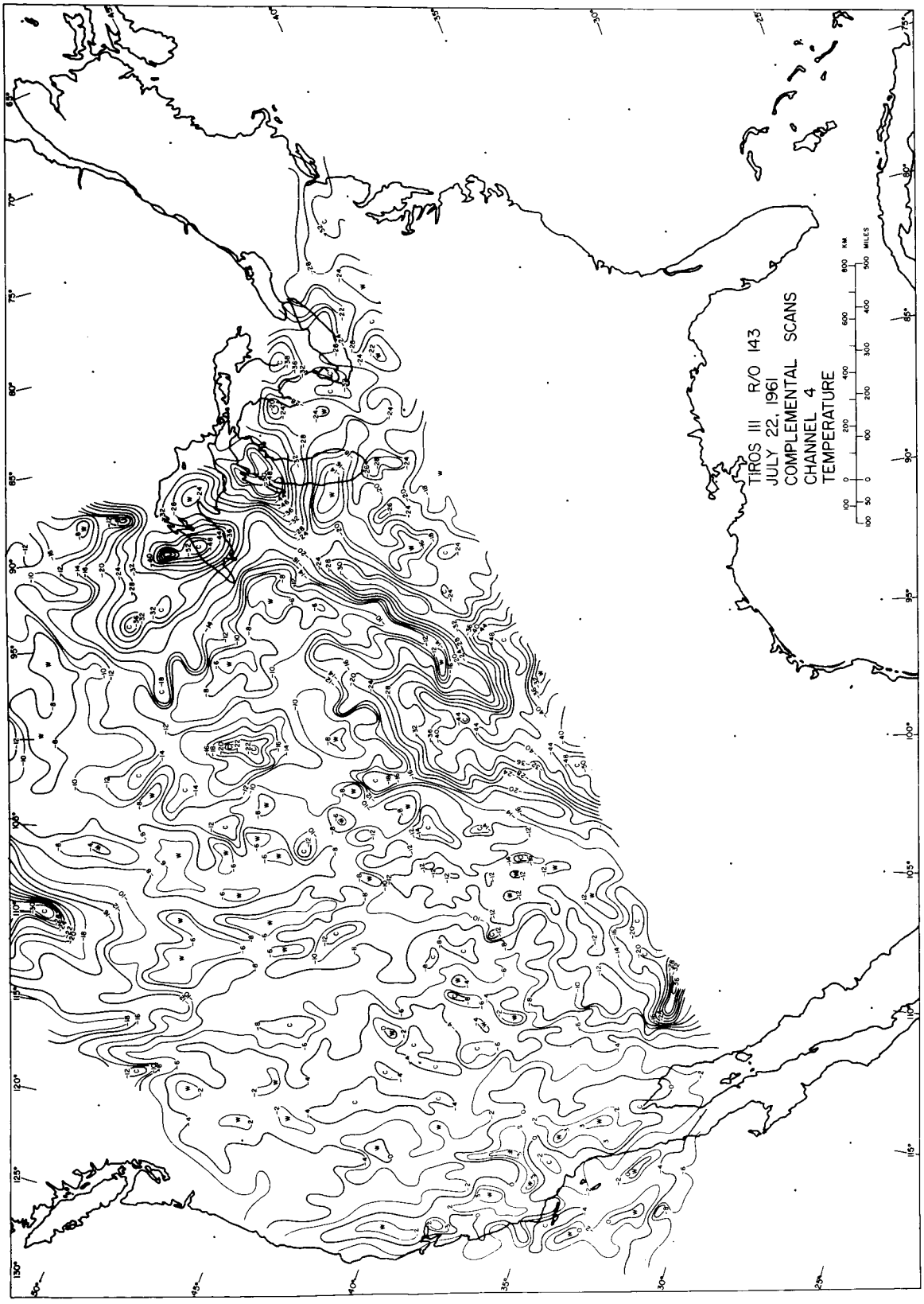

Fig. 10 Effective black-body temperatures. Orbit 143, Channel 4 complemental scans.

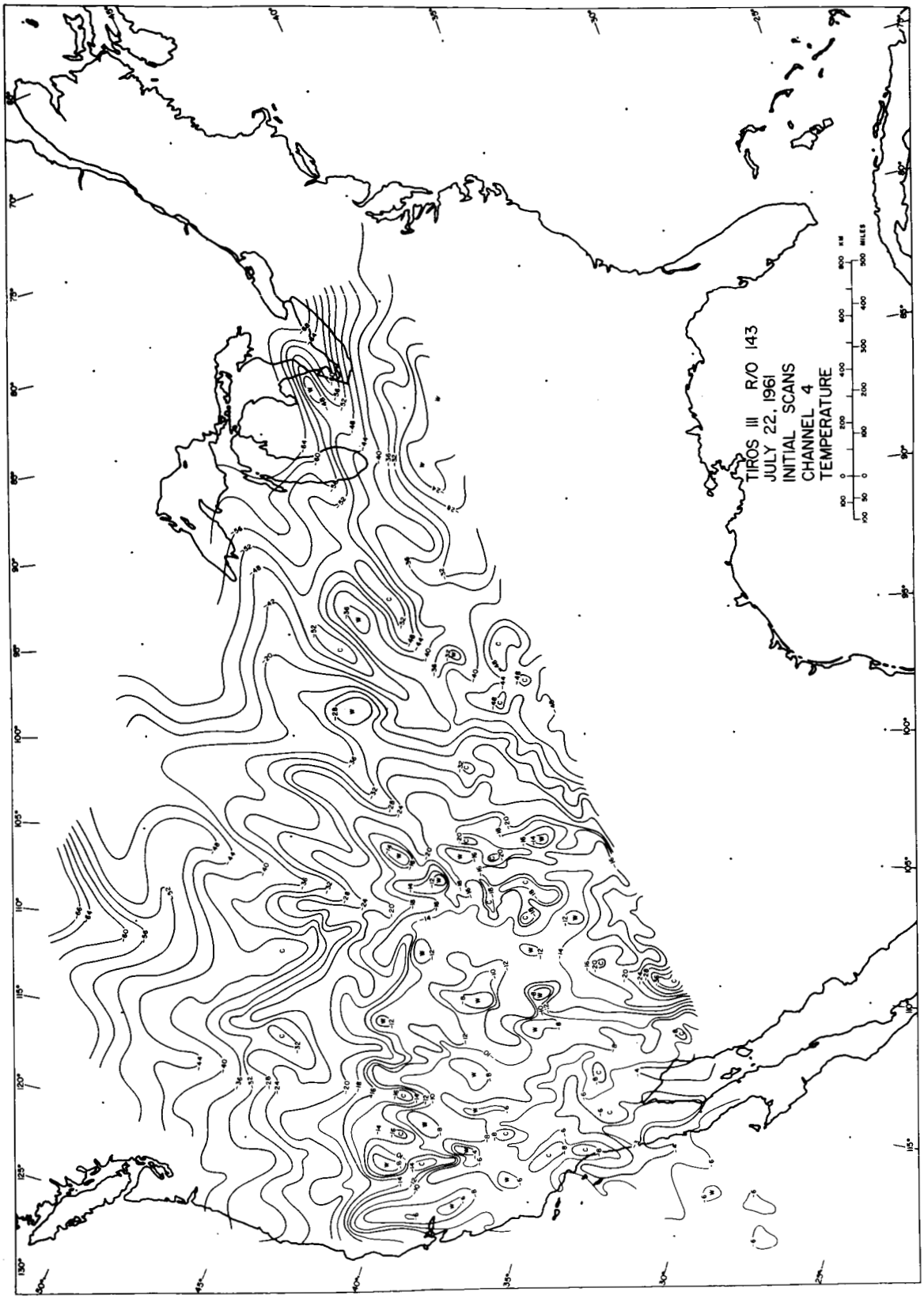

Fig. 11 Effective black-body temperatures. Orbit 143, Channel 4 initial scans.

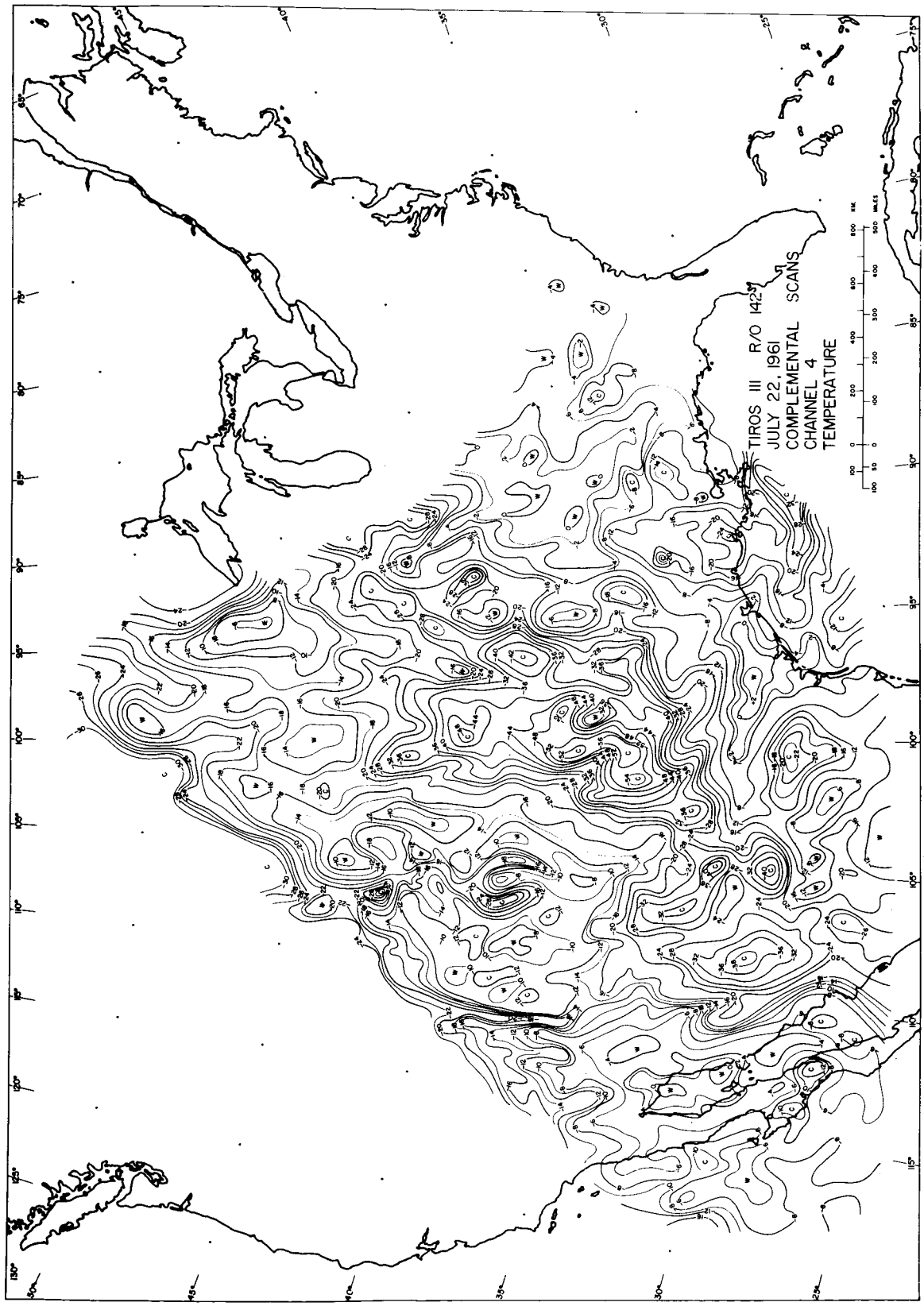

Fig. 12 Effective black-body temperatures. Orbit 142, Channel 4 complemental scans.

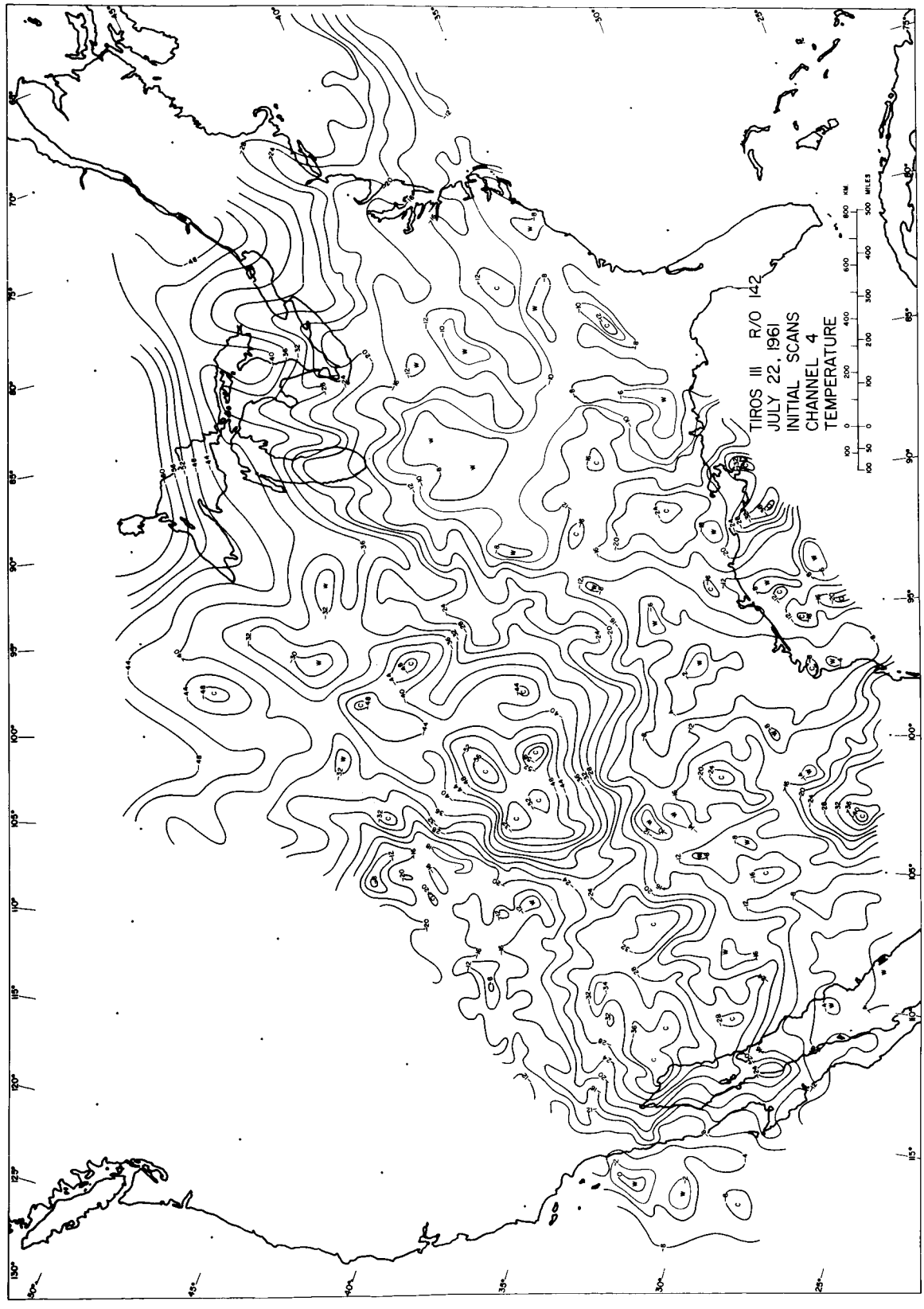

Fig. 13 Effective black-body temperatures. Orbit 142, Channel 4 initial scans.

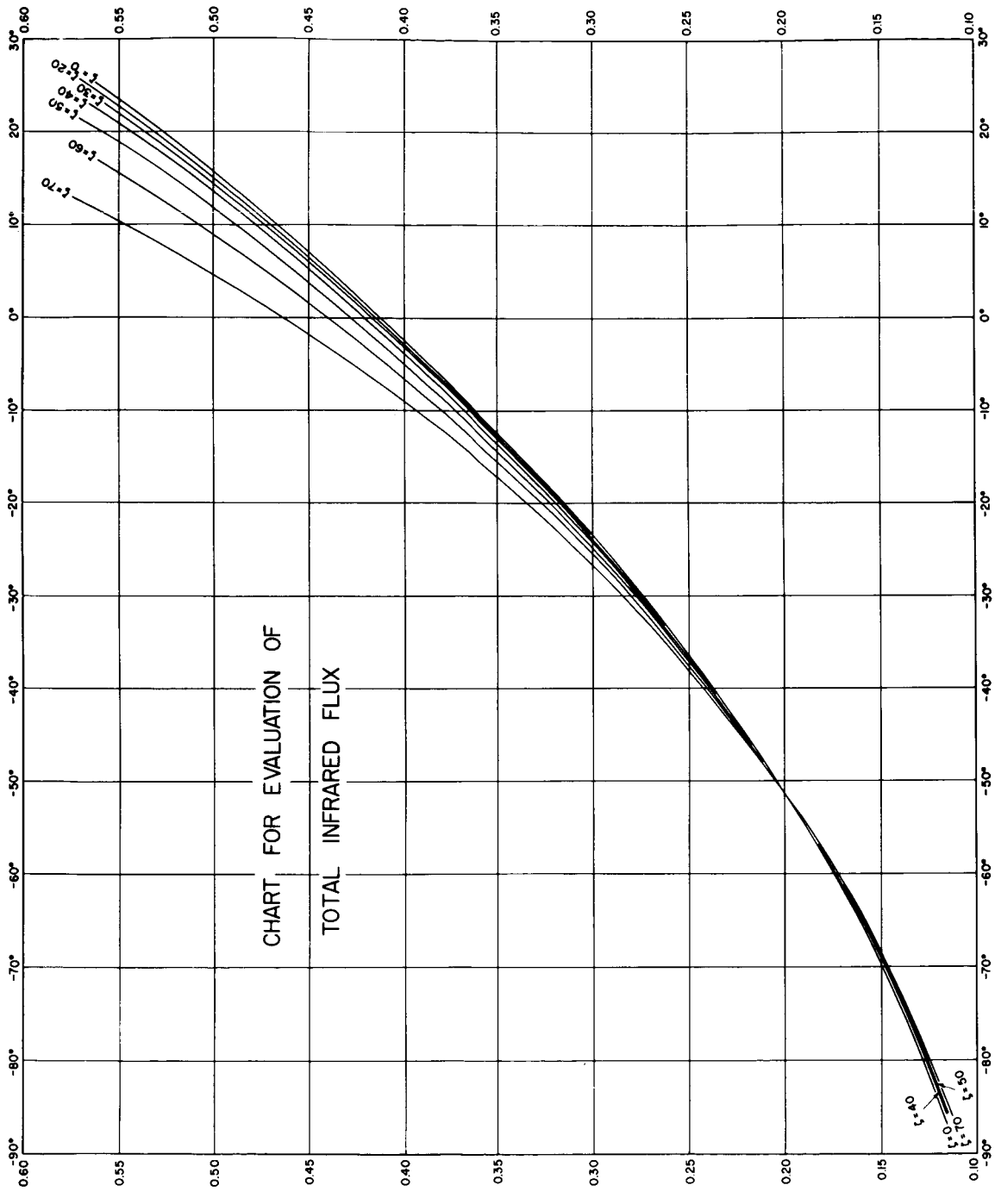

Fig. 14 Total infrared fluxes as function of Channel 4 effective black-body temperatures for various zenith angles.

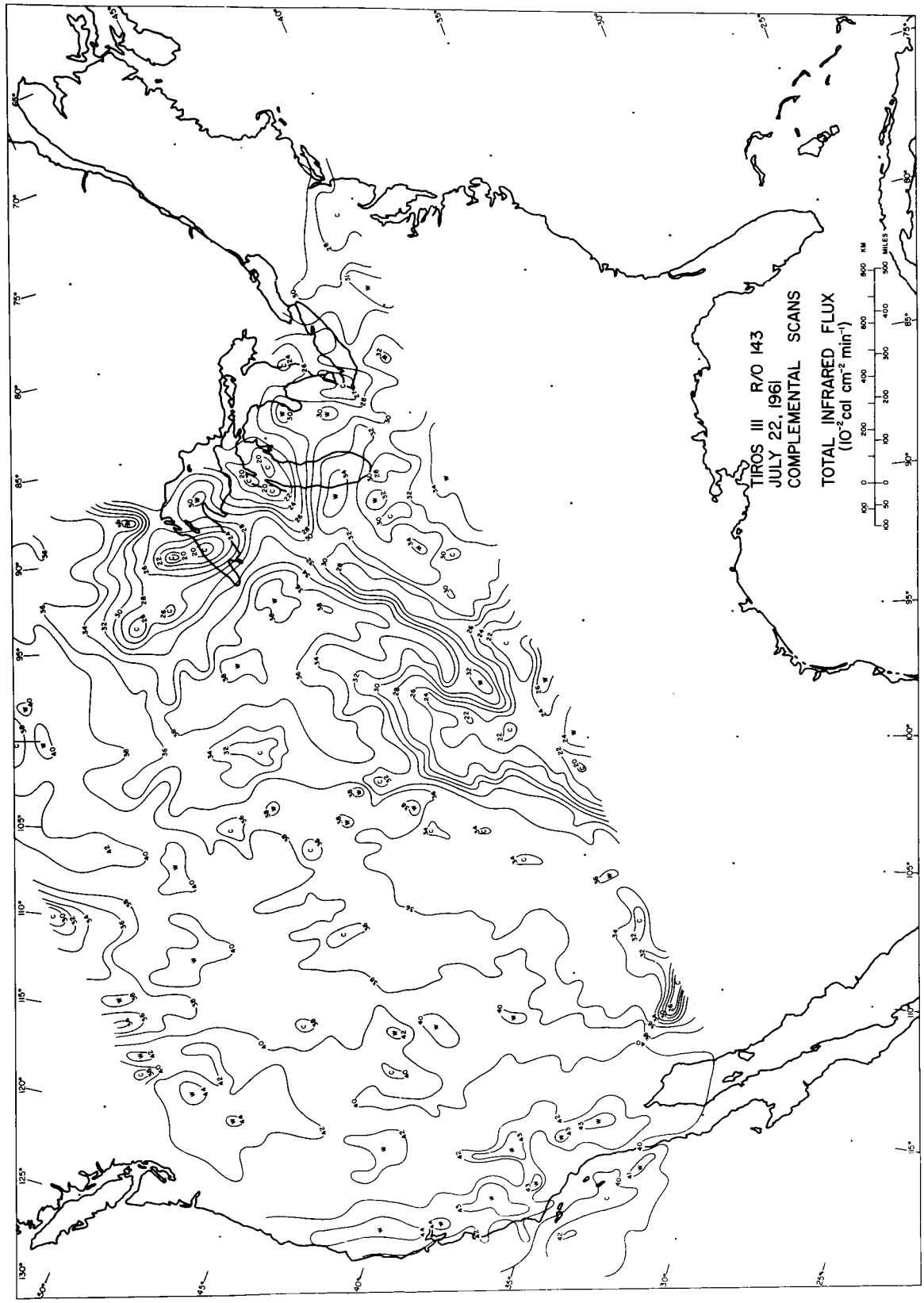

Fig. 15 Outgoing total infrared fluxes. Orbit 143 complemental scans.

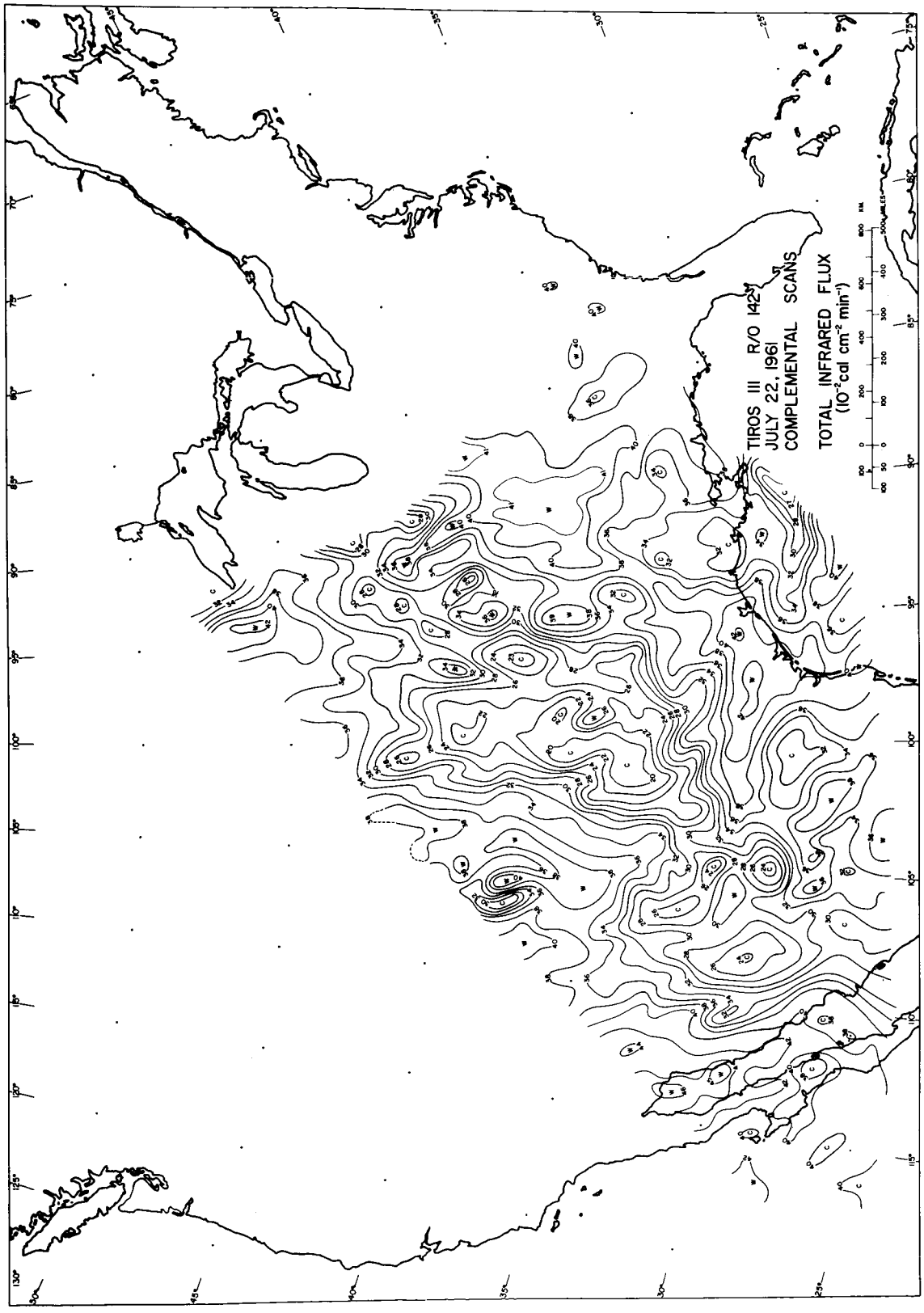

Fig. 16 Outgoing total infrared fluxes. Orbit 142 complemental scans.

MESOMETEOROLOGY PROJECT------- RESEARCH PAPERS

(Continued from front cover)

16. Preliminary Result of Analysis of the Cumulonimbus Cloud of April 21, 1961 - Tetsuya Fujita and James Arnold

17. A Technique for Precise Analysis of Satellite Photographs - Tetsuya Fujita

18. Evaluation of Limb Darkening From TIROS III Radiation Data - S. H. H. Larsen, Tetsuya Fujita, and W. L. Fletcher